Photocatalytic degradation of reactive black 5 on the surface of tin oxide microrods

Shanza Rauf Khan, Muhammad Umar Khalid, Saba Jamil, Songnan Li, Aiman Mujahid and Muhammad Ramzan Saeed Ashraf Janjua

ABSTRACT

A simple co-precipitation technique is proposed for synthesis of tin oxide (SnO_2) microrods. Stannous chloride and urea were used during synthesis. X-ray powder diffraction (XRD) analysis revealed that the annealed product consists of SnO_2 microrods having tetragonal unit cells, while scanning electron microscopy (SEM) analysis revealed the rod-like morphology of a synthesized product. These synthesized microrods are used as photocatalyst for the degradation of reactive black 5 (RB5). Degradation kinetics of RB5 are monitored under daylight in different concentrations of hydrogen peroxide (H_2O_2) and catalyst. The percentage of RB5 conversion is also calculated at various concentrations of hydrogen peroxide and catalyst which demonstrate that RB5 shows high catalytic degradation at high concentrations of hydrogen peroxide and catalyst.

Key words | azo dye, microrods, photocatalyst, reactive black 5, tin oxide

Shanza Rauf Khan (corresponding author)
Muhammad Umar Khalid
Saba Jamil
Aiman Mujahid
Department of Chemistry,
University of Agriculture,
Faisalabad 38000,
Pakistan
E-mail: *shanzaraufkhan@gmail.com*

Songnan Li
Harbin Normal University (Songbei),
Harbin 150025,
China

Muhammad Ramzan Saeed Ashraf Janjua
Department of Chemistry,
King Fahd University of Petroleum and Minerals,
Dhahran 31261,
Saudi Arabia
and
Department of Chemistry,
University of Sargodha,
Sargodha 40100,
Pakistan

INTRODUCTION

Industries contribute greatly to the contamination of water resources. A wide range of hazardous toxic substances are continually released into the water body of the environment due to a lack of effective source treatment techniques. Synthetic dyes play a major role in the contamination of water through industrial waste. These dyes show stable behavior because of their aromatic structures, so synthetic dyes cannot be easily degraded. Their stable structure prevents the absorbance and reflection of sunlight. These dyes are also mutagenic and toxic in nature. Their direct release into the ecosystem disturbs its balance, therefore removal of these synthetic dyes from water resources is necessary to avoid these effects (Chowdhury & Balasubramanian 2014). Photocatalysis plays an important role in the purification of water by removing the biological and chemical contaminants from water resources. Photocatalysis also causes the breakdown of organic contaminants into mineral salts (Wang *et al.* 2006). In a photocatalytic reaction, an electron-hole pair is created with the help of a catalyst which further generates free radicals. These free radicals break down the aromatic structure of dye molecules (Julkapli & Bagheri 2014). Semiconductor materials are used as photocatalyst to remove the dyes from water resources because they can efficiently oxidize organic substances. Semiconductor materials are used as photocatalysts in various fields (hydrogen gas production (Yoong *et al.* 2009), water splitting (Zou *et al.* 2001), dismantling of micro-organisms such as bacteria (Robertson *et al.* 2012), degradation of organic dyes (Chakrabarti & Dutta 2004)). Photons activate electron-hole recombination and the wide energy gap between conduction and valence band in these materials hinders this photo activation (Li & Li 2001). Various organic dyes have been degraded by different semiconductor materials such as zinc oxide (ZnO) (Daneshvar *et al.* 2004; Jamil *et al.* 2017a,

doi: 10.2166/wh.2018.033

2017b), titanium dioxide (TiO_2) (Khataee & Kasiri 2010), tungsten trioxide (WO_3) (Kim *et al.* 2010), cobalt oxide (Co_3O_4) (Dong *et al.* 2007; Jamil *et al.* 2017a, 2017b), ferric oxide (Fe_2O_3) (Cao & Zhu 2008; Janjua *et al.* 2017), copper oxide (Cu_2O) (Yang *et al.* 2006) and tin oxide (SnO_2) (Khalid *et al.* 2018). Recently, the focus on tin oxide has increased because of its applications in various fields as a gas sensor (Leite *et al.* 2000), catalyst (Jiang *et al.* 2005), electrode (Zhu *et al.* 2000), transistor (Shin *et al.* 2011), photovoltaic device (Rajesh *et al.* 2014) and liquid crystal (Demir-Cakan *et al.* 2008). Tin oxide is the most important material because of its strong chemical and physical interaction with absorbed species, high transparency in visible spectrum, strong thermal stability in air and low operating temperature. Tin oxide is available in +2 and +4 oxidation states, so two types of oxides are formed (stannous oxide SnO and stannic oxide SnO_2) (Ge *et al.* 2006). However, among these two oxides, SnO_2 has received attention due to its n-type semiconductor behavior, wide energy gap of 3.6 eV, chemical and mechanical stability and high mobility of electrons (Tazikeh *et al.* 2014). Researchers have a great interest in the synthesis of SnO_2 nano and micro particles by various methods such as sol gel (Gu *et al.* 2004), hydrothermal (Chiu & Yeh 2007; Khalid *et al.* 2018), solvothermal (Anandan & Rajendran 2010), microwave method (Subramanian *et al.* 2008), mechano-chemical (Kersen 2002) and co-precipitation method (Bouaine *et al.* 2007). So the co-precipitation method is chosen for the synthesis of SnO_2 microparticles because it is inexpensive and simple. This method also gives highly crystalline microparticles without using any surfactant and binding species. Using this method shape and size can be easily controlled by changing the concentration of precipitating reagent and precursor salt, pH of medium and reaction temperature. Khan *et al.* (2017) synthesized the ferric oxide (Fe_2O_3) nanorods by a reflux assisted co-precipitation method. Nadaf & Venkatesh (2016) used a co-precipitation technique for the synthesis of SnO_2 nanoparticles. Babar *et al.* (2010) synthesized the nano-crystalline SnO_2 by a co-precipitation method. Nejati-Moghadam *et al.* (2015) fabricated SnO_2 nano structures by a co-precipitation approach. In the present work rod like highly crystalline SnO_2 microparticles are synthesized via a simple co-precipitation approach from a stannous chloride precursor. The product is analyzed using X-ray powder diffraction (XRD) and scanning electron microscopy (SEM) technique. Photocatalytic application of the synthesized product for degradation of reactive black dye 5 from aqueous water is studied.

METHODS

Materials

Hydrated stannous chloride ($SnCl_2.2H_2O$), urea (N_2H_4CO), reactive black 5 dye (RB5) and hydrogen peroxide (H_2O_2) were purchased from Sigma-Aldrich, USA. Distilled water was used throughout the synthesis and catalytic study. All the chemicals were used as such without any further purification.

Synthesis of SnO_2 microrods

SnO_2 microrods were synthesized by the co-precipitation method. The pH of hydrated stannous chloride solution (1 M) was adjusted to 9 using 2 M urea solution under constant stirring at room temperature. The resultant solution was further stirred for 1 h at room temperature. Obtained precipitates were then collected by means of centrifugation and repeatedly washed with ethanol and distilled water and the precipitates were dried in a thermoelectric oven at 80 °C for 24 h. The dried product was ground to powder form and subjected to calcination in an electric furnace at 600 °C for 4 h in the presence of air. Calcined product was subjected to characterization.

Photocatalytic degradation of RB5

RB5 dye, catalyst and H_2O_2 were added to a beaker in the presence of sunlight. After short time intervals, a small amount of sample mixture was taken in a glass cuvette and its spectra scanned on a Halo DB 20 double beam UV-Visible spectrophotometer at 350–800 nm wavelength range. The photocatalytic reduction of RB5 was studied by changing the amount of catalyst dosage and H_2O_2 concentration.

Characterization

A Jeol JDX- 3532 X-ray powder diffractometer was used for XRD analysis. A pattern was recorded in 2θ, range 10–80°. The diffractometer was operated at 45 kV voltage and 40 mA current. A Quanta 250 scanning electron microscope was used for SEM observations at 30 kV voltage. Photocatalytic degradation of RB5 was studied with a Halo DB 20 double beam spectrophotometer.

RESULTS AND DISCUSSION

X-ray powder diffraction analysis

The XRD pattern of SnO_2 rods is shown in Figure 1. Strong diffraction peaks are observed at 2-theta values: 26.53, 33.8, 37.89, 51.65, 54.62, 57.76, 61.75, 64.58°. These peaks are associated with different planes (110, 101, 200, 211, 220, 002, 130, 112). The 2-theta values and corresponding planes are characteristic to SnO_2 entry no. 96-153-4786. Diffraction peaks are very sharp which demonstrate that the synthesize SnO_2 is highly crystalline. One small extra peak is also present at 2-Theta value 44.61 °. This peak is due to the presence of moisture in the sample during analysis. Analysis of SnO_2 confirms that it possesses tetragonal crystal lattice with a P 42/m n m space group. The crystal structure of synthesized SnO_2 is shown in Figure 2.

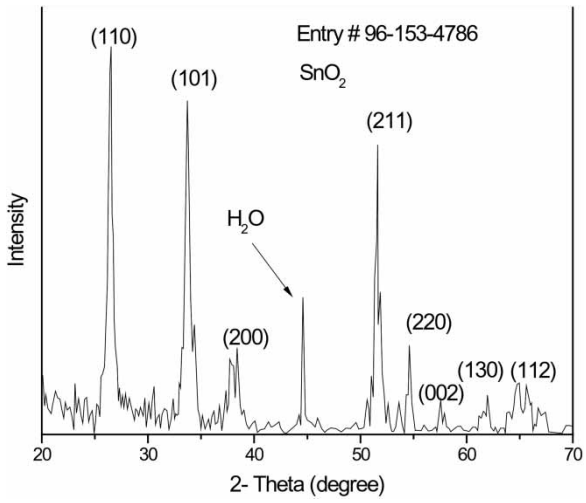

Figure 1 | XRD pattern of synthesized SnO_2 microrods.

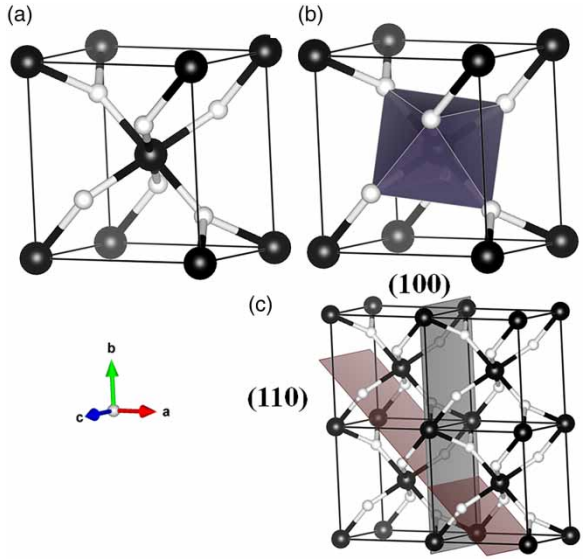

Figure 2 | Structural model of synthesized SnO_2 rods: (a) arrangement of tin and oxygen atoms in tetragonal lattice, (b) formation of octahedron by the coordination of one tin and six oxygen atoms, (c) different planes in tetragonal lattice.

Figure 2(a) shows that tin atoms are located at the corners and body center positions of the crystal lattice and every tin atom is bonded with six oxygen atoms, four of which are at the face of the lattice and two are at the center. Various planes are also shown in Figure 2(c) to reveal the positions of atoms, bond angles and bond lengths.

Scanning electron microscopic analysis

Figure 3 shows the SEM images of SnO_2 microparticles synthesized by a co-precipitation method followed by calcination at 600 °C temperature. It can be seen from Figure 3(a) that the product consists of microrods. The length and diameter of these rods lies in the 6–8 and 0.9–1.7 μm range respectively. Synthesized micro-rods are oriented randomly. Figure 3(b)–3(d) show that the surface of the microrods is not smooth and broken parts of other rods are attached on its surface. Closer analysis of these images reveals that these rod-like structures are formed by self-assembly of needle-like structures. Needle-like structures are arranged parallel to each other and form a rod-like morphology. The diameter of these needle-like structures is around 0.1–0.2 μm. Some irregular shaped small particles are also present along with these rods, which may be the broken parts of other rods.

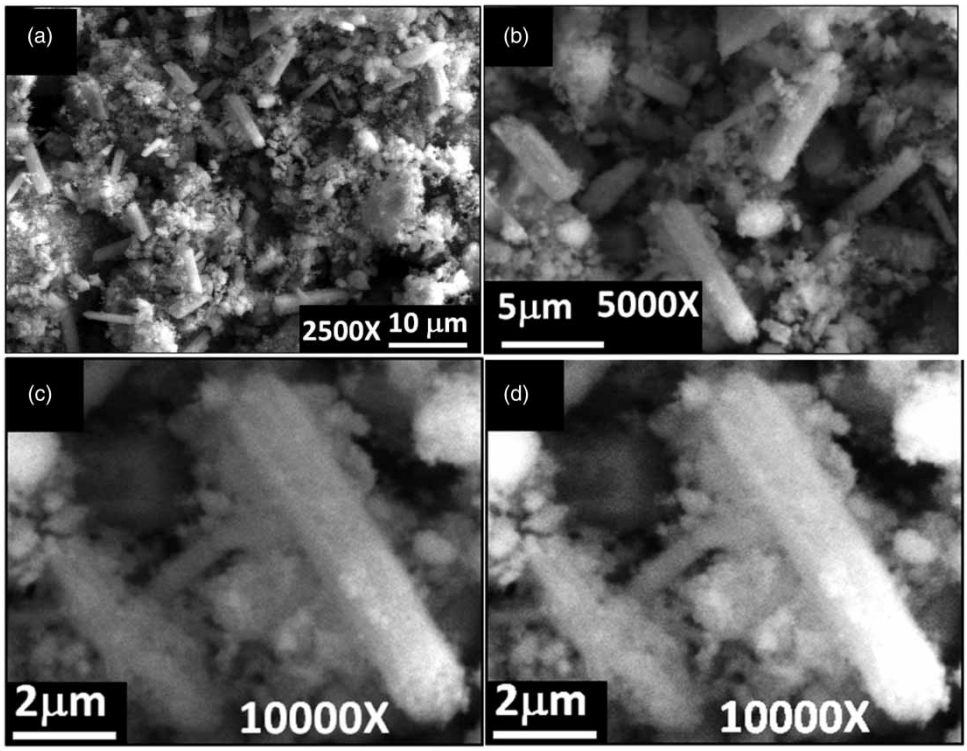

Figure 3 | SEM images of SnO_2 microrods synthesized by co-precipitation technique: (a) overall view of the product, (b) magnified view of product at 5,000×, and (c) and (d) 10,000×.

Formation mechanism

Figure 4 shows the possible formation mechanism of synthesized product which is suggested by XRD and SEM characterizations. Tin (II) oxidizes into tin (IV) in dilute aqueous medium. On the other hand, urea was added into the water which generates the ammonium ions, hydroxyl ions and carbon dioxide in the solution. There are two possible paths now: (1) carbon dioxide can react with hydroxyl ions and produce carbonate ions and water, then these carbonate ions react with tin ions and produce tin carbonate; (2) carbon dioxide gas escapes from the solvent and hydroxyl ions react with tin ions and produce tin hydroxide. The obtained product was calcined at 600 °C and then its XRD pattern was recorded. XRD analysis confirms that the product is SnO_2. It is well known that tin carbonate is

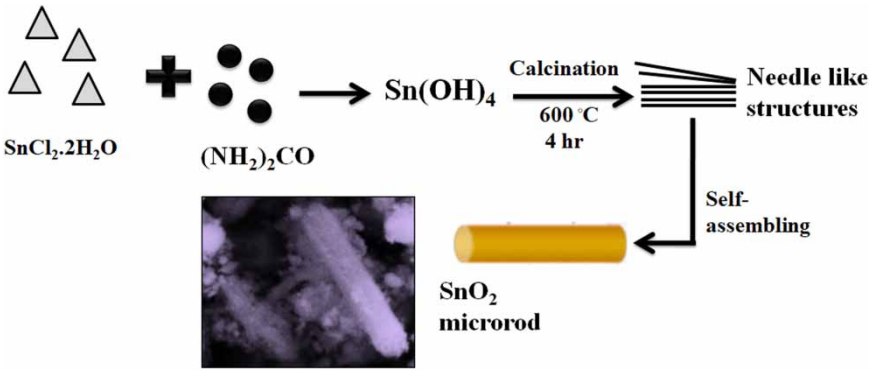

Figure 4 | Formation mechanism of SnO_2 microrods.

stable at 600 °C while tin hydroxide is decomposed into SnO_2 at this temperature. Thus XRD analysis confirms that the reaction has progressed through Path-2. The reaction of hydroxyl ions with tin ions is faster than the reaction of hydroxyl ions with carbon dioxide, therefore Path-2 is favored over Path-1.

When urea solution was added into the stannous chloride solution, tin hydroxide was formed along with ammonium chloride. Formed tin hydroxide ($Sn(OH)_4$) may contain some impurities (chloride ions). These impurities were removed through washing to obtain pure tin hydroxide. Synthesized tin hydroxide was calcined at 600 °C for 4 h which causes the removal of water molecules and dehydration of tin hydroxide into SnO_2. XRD patterns confirm that the synthesized product is SnO_2 microrods. The possible chemical Equations (1)–(7) are given below:

$$SnCl_2 \rightleftarrows Sn^{2+} + 2Cl^- \quad (1)$$

$$Sn^{2+} \rightarrow Sn^{4+} + 2e^- \quad (2)$$

$$NH_2CONH_2 + H_2O \rightarrow CO_2 + 2NH_3 \quad (3)$$

$$H_2O + NH_3 \rightarrow NH_4OH \rightleftarrows NH_4^+ + OH^- \quad (4)$$

$$NH_4^+ + Cl^- \rightarrow NH_4Cl \quad (5)$$

$$Sn^{4+} + 4OH^- \rightarrow Sn(OH)_4 \quad (6)$$

$$Sn(OH)_4 \xrightarrow[4\ hr]{600^\circ C} SnO_2 + 2H_2O \quad (7)$$

Photocatalytic degradation of reactive black 5

Azo dyes characterized by azo group (–N = N–) are the largest class of dyes that are used for dyeing natural and synthetic materials. Among all azo dyes (metal complex, reactive, direct, acidic, basic and sulfur), the most commonly used dyes are reactive type azo dyes. These reactive azo dyes produce water pollution. This is due to the fact that almost 20% of these dyes drained into water streams during the dyeing processes (Lucas *et al.* 2013; Ramesh *et al.* 2016). RB5 is a reactive azo dye and is commonly used in dying industries. RB5 contains highly reactive chromophoric groups such as anthraquinone, azo, oxazine and formazan. These groups can form the covalent bond with fiber. Moreover, due to the complex structure and high chemical stability of RB5, it is very difficult to degrade RB5 from water. RB5 can cause damage to the aquatic environment by preventing the light absorption and photosynthesis process. Furthermore, RB5 is toxic to some organisms and causes the death of these organisms in water. RB5 can be degraded through microorganisms by the breakage of azo bonds but this process causes production of some toxic derivatives (like phenol) which have a carcinogenic and mutagenic effect on human health. Products 2-(ethylthio)-ethyl ester and tert-butyl-N-hydroxycarbamate are produced due to photocatalytic degradation of RB5 (Garg *et al.* 2016). These products are not carcinogenic and aromatic. Moreover, these products are not resistant to environmental conditions, so they easily break down further into smaller molecules. Lambda max (λ_{max}) of RB5 is 590 nm. Figure 5 possesses only one peak at 590 nm which shows that no product is produced during catalysis which is absorbed in the UV-Visible range. All the aromatic and conjugated compounds absorb in this wavelength range. This favors the results obtained by Garg *et al.* (2016). Thus toxic dye is converted into less harmful substances via photocatalysis by micro particles, and this technology can be used for water treatment. Photocatalytic reduction of RB5 on SnO_2 microrod surfaces was chosen as the model reaction (Zielińska *et al.* 2001; Kunz *et al.* 2002; El Bouraie & El Din 2016). The degradation of RB5 was studied by monitoring variation in absorbance at 590 nm wavelength using a UV-Visible spectrophotometer. The UV-Visible spectra of photocatalytic reduction of RB5 in the absence and presence of catalyst is shown in Figure 5(a) and 5(b) respectively. Spectra were scanned at different time intervals. It is observed from Figure 5(a) that absorbance at 590 nm does not decrease, even after 120 min, which indicates that the dye is not degraded, while Figure 5(b) shows that at the start of catalysis, absorbance at 590 nm was 0.48. However, with the passage of time, absorbance at 590 nm decreases. This shows that he concentration of dye is continuously decreasing in the mixture which confirms that the catalyst is performing its role and dye degradation does not occur in the absence of catalyst. The absorbance sharply decreases until 30 min after sunlight irradiation. After 30 min, absorbance at 590 nm decreases slowly with time which indicates that the degradation reaction is near

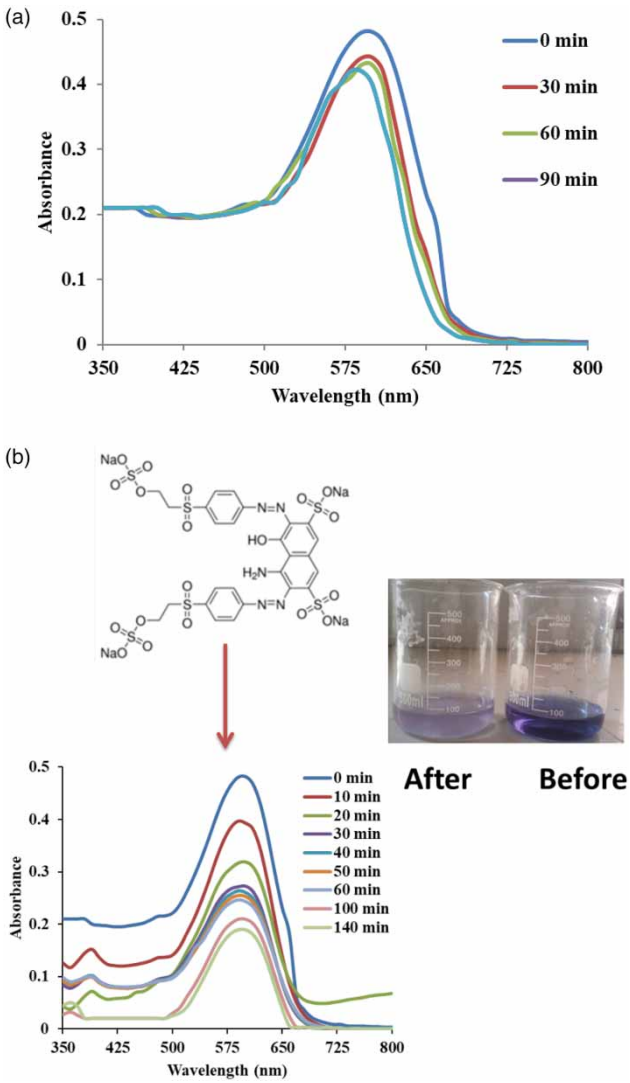

Figure 5 | UV–Vis spectra of the photocatalytic reduction of RB5 dye under daylight at various time intervals: (a) in the absence of catalyst and (b) in the presence of 0.35 mg/mL catalyst dosage (conditions: [RB5] = 10 ppm and $[H_2O_2] = 0.1$ M).

completion. The color of RB5 is changed from dark blue to light blue which also reveals that the concentration of dye is decreased in the reaction mixture.

Effect of catalyst dosage on catalytic degradation of RB5 dye

Figure 6 shows the plot of ln (A_t/A_o) versus time for various catalyst dosages (0.35, 0.69 and 1.0 mg/mL). In all graphs at the start of the reaction the change in values of ln (A_t/A_o) is very fast and gives linear behavior. This linear portion of the

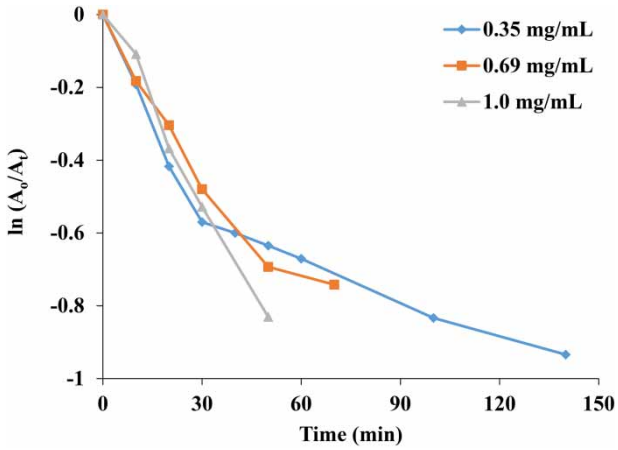

Figure 6 | Plot of ln (A_t/A_o) versus time for photocatalytic reduction of RB5 under various catalyst dosages (conditions: [RB] = 10 ppm, $[H_2O_2] = 0.1$ M, [catalyst] = 0.35, 0.69 and 1.0 mg/mL).

plots is used to calculate the values of k_{aap}, however, after some time these values decrease slowly. The slope of these plots is different, which suggests that the degradation rate is not the same under different dosages of catalyst. The small value of ln (A_t/A_o) at 0.35 mg/mL catalyst dosage suggests that the catalysis rate is very slow in the case of low concentrations of catalyst (0.35 mg/mL). The plot between k_{aap} and catalyst dosage is shown in Figure 7. It is seen that the values of k_{aap} increase by increasing the catalyst dosage. The value of k_{app} is found to be 0.0138, 0.0158 and 0.0175 min^{-1} at 0.35, 0.69 and 1.00 mg/mL catalyst dosages respectively (Table S1, available with the online version of this paper). It is observed that the value of k_{app}

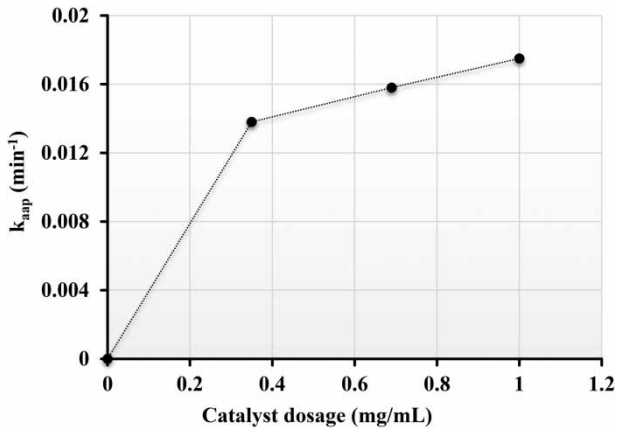

Figure 7 | Plot of k_{aap} versus various catalyst dosage (conditions: [RB5] = 10 ppm, $[H_2O_2] = 0.1$ M, [catalyst] = 0.35, 0.69 and 1.0 mg/mL).

increases sharply with an increase in catalyst dosage from 0 to 0.35 mg/mL. A further increase in concentration of catalyst from 0.35 to 1.00 mg/mL does not largely affect the value of k_{aap}. Actually, the catalyst provides active sites for the adsorption of dye molecules. As the concentration of catalyst dosage increases, it causes an increase in available active sites, so a greater number of dye molecules can adsorb on the surface of the catalyst and the rate of photocatalytic degradation increases.

Effect of concentration of H_2O_2 on degradation of RB5

Figure S1 (available online) shows the plot of ln (A_t/A_o) versus time for different concentrations of H_2O_2 (0.1, 0.4 and 0.7 M). It can be seen from the plot that at the start of the reaction the value of ln (A_t/A_o) decreases very fast and shows linear behavior. However, after some time the value of ln (A_t/A_o) decreases slowly with time in the case of 0.1 M concentration of H_2O_2. The plot between k_{aap} and various concentrations of H_2O_2 is shown in Figure 8. This plot shows that the k_{app} reaction increases by increasing the concentration of H_2O_2. As H_2O_2 concentration increases from 0.1 to 0.7 M, the value of k_{aap} also increases from 0.0158 to 0.0266 min^{-1}. Figure 8 also shows that the value of k_{app} does not linearly increase with an increase in concentration of H_2O_2. H_2O_2 donates oxidizing species hydroxyl radical (·OH) which contributes to the degradation process. By increasing the concentration of the H_2O_2 amount of oxidizing species, ·OH increases which helps to rapidly degrade dye molecules and catalysis rate increases.

Percentage conversion of RB5

The comparison of percentage conversion of RB5 at various concentrations of H_2O_2 (0.1, 0.4 and 0.7 M) and catalyst (0.35, 0.69 and 1.0 mg/mL) is shown in Figure 9. It is clear from Figure 9 that at low concentrations of H_2O_2 (0.1 M) and catalyst (0.35 mg/mL) the percentage conversion of RB5 is also low (72%). However, as the concentration of H_2O_2 increases from 0.1 to 0.4 M, the percentage conversion of dye also increases (76%) and the dye shows maximum percentage conversion (82%) at higher concentrations (0.7 M) of H_2O_2. The same behavior is seen in the case of catalyst dosage. By increasing the amount of catalyst from 0.35 to 0.69 mg/mL, percentage conversion of RB5 increases to 81% and it reaches the maximum value of 84% at higher catalyst dosages (1.0 mg/mL). The data of percentage conversion of RB5 under studied conditions of H_2O_2 and catalyst dosage show that maximum degradation occurs when 0.7 M H_2O_2 and 1.0 mg/mL catalyst is used. This also shows that the catalyst has the ability to rapidly degrade the dye with high percentage conversion. Researchers used various semiconductor materials for the RB5. Lucas *et al.* (2013) achieved 91% degradation efficiency of RB5 by using TiO_2 coated magnetic nanoparticles. Wong *et al.* (2015) used the reduced graphene oxide for the reduction of RB5 and they achieved 49% decolonization of RB5 under UV irradiation. Soo *et al.* (2016) used the Fe-doped mesoporous

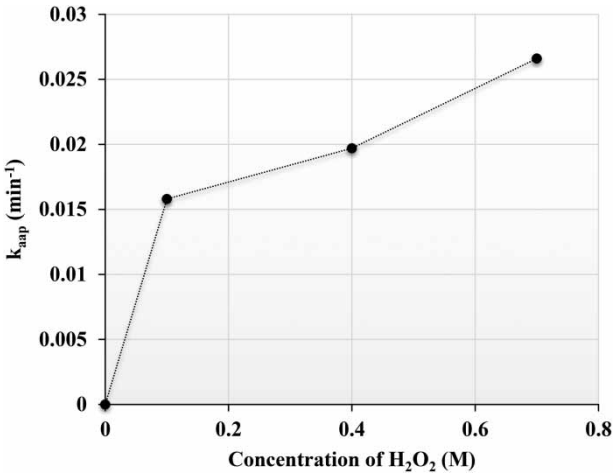

Figure 8 | Plot of k_{aap} versus various concentrations of H_2O_2 (conditions: [RB5] = 10 ppm, $[H_2O_2]$ = 0.1, 0.4 and 0.7 M and [catalyst] = 0.35 mg/mL).

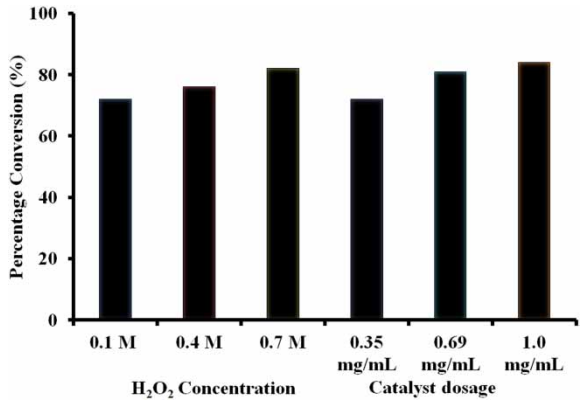

Figure 9 | Percentage conversion of RB5 dyes under various concentrations of H_2O_2 and catalyst dosage.

TiO_2 for the degradation of RB5. From the literature it is seen that no one used the SnO_2 microparticles for the reduction of RB5. So in this work, the catalytic effect of SnO_2 microrods for the reduction of RB5 from wastewater is investigated.

CONCLUSIONS

SnO_2 microrods are synthesized by the co-precipitation method followed by calcination at 600 °C temperature. XRD analysis confirms the formation of high crystalline SnO_2. It also reveals that every tin atom is bonded to six oxygen atoms. Oxygen atoms are present at the octahedral position around the tin central atom. Morphological analysis confirms the formation of microrods whose diameter and length are in the range of 6–8 and 0.9–1.7 μm, respectively. Degradation of RB5 is studied to check the photocatalytic behavior of synthesized SnO_2 microrods. The apparent rate constant (k_{app}) values increase by increasing the H_2O_2 concentration and amount catalyst. Percentage conversion of RB5 is also calculated which revealed that at low H_2O_2 concentration (0.1 M) and catalyst dosage (0.35 mg/mL), percentage degradation of dye is also small (72%). However, as the dosage of catalyst increases from 0.35 to 1.0 mg/mL, the percentage degradation of dye also increases from 72 to 84%. Similarly, the percentage removal of dye from the reaction mixture increases from 72%, and 82% with an increase in concentration of H_2O_2 from 0.1 to 0.7 M. These results indicate that synthesized SnO_2 microrods possess good photocatalytic properties.

ACKNOWLEDGEMENTS

The authors are very grateful to the Department of Chemistry, University of Agriculture, Faisalabad 38000, Pakistan for financial assistance.

REFERENCES

Anandan, K. & Rajendran, V. 2010 Size controlled synthesis of SnO_2 nanoparticles: facile solvothermal process. *J. Non-Oxide Glass.* **2**, 83–89.

Babar, A., Shinde, S., Moholkar, A. & Rajpure, K. 2010 Electrical and dielectric properties of co-precipitated nanocrystalline tin oxide. *J. Alloys Compd.* **505**, 743–749.

Bouaine, A., Brihi, N., Schmerber, G., Ulhaq-Bouillet, C., Colis, S. & Dinia, A. 2007 Structural, optical, and magnetic properties of Co-doped SnO_2 powders synthesized by the coprecipitation technique. *J. Phys. Chem. C* **111**, 2924–2928.

Cao, S. W. & Zhu, Y. J. 2008 Hierarchically nanostructured α-Fe_2O_3 hollow spheres: preparation, growth mechanism, photocatalytic property, and application in water treatment. *J. Phys. Chem. C* **112**, 6253–6257.

Chakrabarti, S. & Dutta, B. K. 2004 Photocatalytic degradation of model textile dyes in wastewater using ZnO as semiconductor catalyst. *J. Hazard. Mater.* **112**, 269–278.

Chiu, H. C. & Yeh, C. S. 2007 Hydrothermal synthesis of SnO_2 nanoparticles and their gas-sensing of alcohol. *J. Phys. Chem. C* **111**, 7256–7259.

Chowdhury, S. & Balasubramanian, R. 2014 Graphene/semiconductor nanocomposites (GSNs) for heterogeneous photocatalytic decolorization of wastewaters contaminated with synthetic dyes: a review. *Appl. Catal. B* **160**, 307–324.

Daneshvar, N., Salari, D. & Khataee, A. 2004 Photocatalytic degradation of azo dye acid red 14 in water on ZnO as an alternative catalyst to TiO_2. *J. Photochem. Photobiol. A Chem.* **162**, 317–322.

Demir-Cakan, R., Hu, Y.-S., Antonietti, M., Maier, J. & Titirici, M.-M. 2008 Facile one-pot synthesis of mesoporous SnO_2 microspheres via nanoparticles assembly and lithium storage properties. *Chem. Mater.* **20**, 1227–1229.

Dong, Y., He, K., Yin, L. & Zhang, A. 2007 A facile route to controlled synthesis of Co_3O_4 nanoparticles and their environmental catalytic properties. *Nanotechnology* **18**, 435602.

El Bouraie, M. & El Din, W. S. 2016 Biodegradation of Reactive Black 5 by *Aeromonas hydrophila* strain isolated from dye-contaminated textile wastewater. *Sustain. Environ. Res.* **26**, 209–216.

Garg, A., Sangal, V. K. & Bajpai, P. K. 2016 Decolorization and degradation of reactive black 5 dye by photocatalysis: modeling, optimization and kinetic study. *Desal. Water Treat.* **57**, 18003–18015.

Ge, J. P., Wang, J., Zhang, H. X., Wang, X., Peng, Q. & Li, Y. D. 2006 High ethanol sensitive SnO_2 microspheres. *Sens. Actuators B* **113**, 937–943.

Gu, F., Wang, S. F., Lü, M. K., Zhou, G. J., Xu, D. & Yuan, D. R. 2004 Photoluminescence properties of SnO_2 nanoparticles synthesized by sol-gel method. *J. Phys. Chem. B* **108**, 8119–8123.

Jamil, S., Janjua, M. R. S. A. & Khan, S. R. 2017a Synthesis of self-assembled Co_3O_4 nanoparticles with porous sea urchin-like morphology and their catalytic and electrochemical applications. *Aust. J. Chem.* **70**, 908–916.

Jamil, S., Janjua, M. R. S. A., Khan, S. R. & Jahan, N. 2017b Synthesis, characterization and catalytic application of polyhedron zinc oxide microparticles. *Mater. Res. Express* **4**, 015902–015910.

Janjua, M. R. S. A., Jamil, S., Jahan, N., Khan, S. R. & Mirza, S. 2017 Morphologically controlled synthesis of ferric oxide nano/micro particles and their catalytic application in dry and wet media: a new approach. *Chem. Cent. J.* **11**, 49.

Jiang, L., Sun, G., Zhou, Z., Sun, S., Wang, Q., Yan, S., Li, H., Tian, J., Guo, J. & Zhou, B. 2005 Size-controllable synthesis of monodispersed SnO_2 nanoparticles and application in electrocatalysts. *J. Phys. Chem. B* **109**, 8774–8778.

Julkapli, N. & Bagheri, S. 2014 Graphene supported heterogeneous catalysts: an overview. *Int. J. Hydrogen Energy* **40**, 948–979.

Kersen, Ü. 2002 The gas-sensing potential of nanocrystalline SnO_2 produced by a mechanochemical milling via centrifugal action. *Appl. Phys. A* **75**, 559–563.

Khalid, M. U., Khan, S. R. & Jamil, S. 2018 Morphologically controlled synthesis of cubes like tin oxide nanoparticles and study of its application as photocatalyst for Congo red degradation and as fuel additive. *J. Inorg. Organomet. Polym. Mater.* **28**, 168–176.

Khan, S. R., Jamil, S., Janjua, M. R. S. A. & Khera, R. A. 2017 Synthesis of ferric oxyhydroxide nanoparticles and ferric oxide nanorods by reflux assisted coprecipitation method and comparative study of their thermal properties. *Mater. Res. Express* **4**, 115019–115025.

Khataee, A. & Kasiri, M. B. 2010 Photocatalytic degradation of organic dyes in the presence of nanostructured titanium dioxide: influence of the chemical structure of dyes. *J. Mol. Catal. A* **328**, 8–26.

Kim, J., Lee, C. W. & Choi, W. 2010 Platinized WO_3 as an environmental photocatalyst that generates OH radicals under visible light. *Environ. Sci. Technol.* **44**, 6849–6854.

Kunz, A., Mansilla, H. & Duran, N. 2002 A degradation and toxicity study of three textile reactive dyes by ozone. *Environ. Technol.* **23**, 911–918.

Leite, E., Weber, I., Longo, E. & Varela, J. A. 2000 A new method to control particle size and particle size distribution of SnO_2 nanoparticles for gas sensor applications. *Adv. Mater.* **12**, 965–968.

Li, X. & Li, F. 2001 Study of Au/Au^{3+}-TiO_2 photocatalysts toward visible photooxidation for water and wastewater treatment. *Environ. Sci. Technol.* **35**, 2381–2387.

Lucas, M. S., Tavares, P. B., Peres, J. A., Faria, J. L., Rocha, M., Pereira, C. & Freire, C. 2013 Photocatalytic degradation of Reactive Black 5 with TiO_2-coated magnetic nanoparticles. *Catal. Today* **209**, 116–121.

Nadaf, L. & Venkatesh, K. 2016 Synthesis and characterization of tin oxide nanoparticles by co-precipitation method. *J. Appl. Chem.* **9**, 1–4.

Nejati-Moghadam, L., Esmaeili Bafghi-Karimabad, A., Salavati-Niasari, M. & Safardoust, H. 2015 Synthesis and characterization of SnO_2 nanostructures prepared by a facile precipitation method. *J. Nanostruct.* **5**, 47–53.

Rajesh, N., Kannan, J., Krishnakumar, T., Leonardi, S. & Neri, G. 2014 Sensing behavior to ethanol of tin oxide nanoparticles prepared by microwave synthesis with different irradiation time. *Sens. Actuators B* **194**, 96–104.

Ramesh, M., Nagaraja, H., Rao, M. P., Anandan, S. & Huang, N. 2016 Fabrication, characterization and catalytic activity of α-MnO_2 nanowires for dye degradation of reactive black 5. *Mater. Lett.* **172**, 85–89.

Robertson, P. K., Robertson, J. M. & Bahnemann, D. W. 2012 Removal of microorganisms and their chemical metabolites from water using semiconductor photocatalysis. *J. Hazard. Mater.* **211**, 161–171.

Shin, G., Yoon, C. H., Bae, M. Y., Kim, Y. C., Hong, S. K., Rogers, J. A. & Ha, J. S. 2011 Stretchable field-effect-transistor array of suspended SnO_2 nanowires. *Small* **7**, 1181–1185.

Soo, C. W., Juan, J. C., Lai, C. W., Hamid, S. B. A. & Yusop, R. M. 2016 Fe-doped mesoporous anatase-brookite titania in the solar-light-induced photodegradation of Reactive Black 5 dye. *J. Taiwan Inst. Chem. Eng.* **68**, 153–161.

Subramanian, V., Burke, W. W., Zhu, H. & Wei, B. 2008 Novel microwave synthesis of nanocrystalline SnO_2 and its electrochemical properties. *J. Phys. Chem. C* **112**, 4550–4556.

Tazikeh, S., Akbari, A., Talebi, A. & Talebi, E. 2014 Synthesis and characterization of tin oxide nanoparticles via the co-precipitation method. *Mater. Sci. Poland* **32**, 98–101.

Wang, G., Lu, W., Li, J., Choi, J., Jeong, Y., Choi, S. Y., Park, J. B., Ryu, M. K. & Lee, K. 2006 V-shaped tin oxide nanostructures featuring a broad photocurrent signal: an effective visible-light-driven photocatalyst. *Small* **2**, 1436–1439.

Wong, C. P. P., Lai, C. W., Lee, K. M. & Hamid, S. B. A. 2015 Advanced chemical reduction of reduced graphene oxide and its photocatalytic activity in degrading reactive black 5. *Materials* **8**, 7118–7128.

Yang, H., Ouyang, J., Tang, A., Xiao, Y., Li, X., Dong, X. & Yu, Y. 2006 Electrochemical synthesis and photocatalytic property of cuprous oxide nanoparticles. *Mater. Res. Bull.* **41**, 1310–1318.

Yoong, L., Chong, F. K. & Dutta, B. K. 2009 Development of copper-doped TiO_2 photocatalyst for hydrogen production under visible light. *Energy* **34**, 1652–1661.

Zhu, J., Lu, Z., Aruna, S., Aurbach, D. & Gedanken, A. 2000 Sonochemical synthesis of SnO_2 nanoparticles and their preliminary study as Li insertion electrodes. *Chem. Mater.* **12**, 2557–2566.

Zielińska, B., Grzechulska, J., Grzmil, B. & Morawski, A. W. 2001 Photocatalytic degradation of reactive black 5: a comparison between TiO_2-Tytanpol A11 and TiO_2-Degussa P25 photocatalysts. *Appl. Catal. B* **35**, L1–L7.

Zou, Z., Ye, J., Sayama, K. & Arakawa, H. 2001 Direct splitting of water under visible light irradiation with an oxide semiconductor photocatalyst. *Nature* **414**, 625–627.

First received 30 January 2018; accepted in revised form 15 June 2018. Available online 11 July 2018